Recycling of Fiberglass Wind Turbine Blades into Reinforced Filaments for use in Additive Manufacturing

Amirmohammad Rahimizadeh[a], Jordan Kalman[b], Kazem Fayazbakhsh[b,*], Larry Lessard[a]

[a] Department of Mechanical Engineering, McGill University, Montreal, QC H3A0C3, Canada

[b] Department of Aerospace Engineering, Ryerson University, Toronto, Ontario M5B2K3, Canada

[*]Corresponding author: kazem@ryerson.ca; Tel: (+1) 416-979-5000 ext. 6414; fax: (+1) 416-979-5056

Abstract

The wind energy industry is one of the fastest-growing application sectors of composites, where reinforcement fibers are used in the manufacturing of light rotor blades. Considering the limited lifetime of turbine blades, a growing number of wind turbines will start to be decommissioned. Turbine blades are generally landfilled at their end-of-life, which highly impacts the environment. This paper proposes a systematic scheme combining mechanical recycling and 3D printing to recycle the valuable constituents of the scrap blades and reuse them in a Fused Filament Fabrication (FFF) process with the aim of improving the mechanical performance of 3D printed components. Mechanical grinding integrated with a double sieving mechanism is utilized to recover the reinforcement fibers. Tensile test specimens with 5 wt% fiber content are fabricated from the recycled fibers and plastic pellets and their mechanical properties as well as internal microstructure are investigated. The results demonstrate an improvement of 16% and 10 % in the elastic modulus and ultimate strength of the reinforced composite filament as compared to the commercially available pure PLA filament. As well, a Young's modulus of 3.35 GPa was observed for the FFF fabricated samples, which is an 8% increase relative to pure PLA samples.

Keywords: A. Wind energy industry, E. Mechanical recycling, E. Fused filament fabrication, B. Mechanical properties

Composites Part B: Engineering

https://doi.org/10.1016/j.compositesb.2019.107101

1. Introduction

The superior mechanical properties of composite materials provide an exiting opportunity to build structures that are lightweight and of high strength, characteristics that have led to many engineering applications for composites [1-4]. The wind energy industry represents one of the fastest growing application sectors of composites, where reinforcement fibers, such as fiberglass or carbon fibers, a plastic polymer, such as polyester or epoxy, and a core material are used to build strong and compliant rotor blades [5]. The dramatic growth of wind industry over the past 20 years has resulted in an extensive amount of end-of-life rotor blades. Current routes to dispose of turbine blades at their end-of-life involve landfill and incineration, methods that are associated with environmental impact [6, 7]. Given the non-biodegradable nature of turbine blades, recent environmental legislation has increasingly demanded for the recycling and replacing of turbine blades in the near future [5, 6, 8]. Recent research efforts in the area of wind energy have been focused on the development of sustainable methods for the recycling and reuse of rotor blades. To address this pivotal challenge, scientists have resorted to chemical and pyrolysis techniques to recover glass fibers from end-of-life turbine blades [6]. Despite the high mechanical properties of the recycled fibers, these techniques show little promise in terms of commercialisation due to the use of hazardous chemicals and/or excessive cost. Mechanical grinding is the only recycling technique, which has found its way to industrial application [9]. Compared to thermal and chemical techniques, this method offers a straightforward and economically feasible scheme for the recycling of composites, particularly glass fiber reinforced materials [10, 11]. A recent research study investigated the feasibility of reusing the mechanically recovered fibers from wind turbines blades to reinforce polypropylene [12]. The results have revealed that the mechanical properties of the recycled composite parts made of the shredded fibers are comparable to those observed for parts made of pyrolyzed fibers. They have also shown that as opposed to pyrolyzed fibers, the shredded glass fibers retain the glass sizing. As a result, mechanical grinding can be considered as a simple and straightforward solution to handle the glass fiber reinforced plastics.

Recent studies have shown that composite materials can be systematically designed and used to produce strong and stiff feedstocks for Additive Manufacturing (AM) processes [13-16]. AM represents a class of fabrication techniques where a layer-upon-layer method is used to build a part from a 3D model [17-19]. AM enables the fabrication of components with complex geometries, those that are unachievable using traditional manufacturing techniques [20]. Fused Filament Fabrication (FFF) is the most widely used 3D printing process due to its simplicity, low cost, and minimal wastage [21]. While extremely efficient, FFF parts are generally made of pure thermoplastic material, which results in low strength and stiffness, dominant factors in contributing to their limited structural performance [22-26]. The mechanical properties of the FFF manufactured parts depend upon a multiple of factors including the filament material, extrusion process of the filament, as well as the manufacturing process and design parameters. Recent advances in AM involve the integration of reinforcing materials with the thermoplastic polymers with the goal of enhancing their mechanical properties. This technique offers the possibility of manufacturing functional parts with strong and stiff microstructure.

Corcione et al. [27] incorporated NanoHydroxyApatite powder into polylactic acid (PLA) to produce b-tricalcium phosphate–based PLA composites as a feedstock material for FFF process. Differential Scanning Calorimetry (DSC) analysis showed promising results in terms of the glass transition temperature of the NanoHA/PLA filament, a crucial factor to the success of the 3D printing process. The newly introduced filament was successfully used to print bone allografts with higher compressive strength relative to those printed using pure PLA filaments. More recently, Kuo et al. [28] attempted to improve the thermomechanical properties of Acrylonitrile butadiene styrene (ABS) filaments using thermoplastic starches (TPS). ABS polymer and TPS agents were used to produce FFF feedstock filaments. In order to increase the processability of the filament, a plasticizer namely, glycerol/water was used. Mechanical and thermal tests performed on the filament showed an improved thermal resistance, heat distortion temperature, flexural modulus, impact strength, tensile strength, and flexural strength. Nikzad et al. [29] postulated that the addition of iron powder into ABS reduce the tensile strength of the filament when compared to pure ABS. Nevertheless, iron/ABS filament exhibited an improved thermal conductivity and heat capacity, which ensured thermally stable 3D printed parts with high dimensional accuracy.

Other strategies that deal with the improvement of FFF 3D printed parts involve the incorporation of reinforcement fibers e.g., carbon and glass fibers, into the polymeric filaments. In one interesting study, Shofner et al. [30] used ABS matrix to develop nano-fiber reinforced composites through FFF. The filament was made of single-walled carbon nanotubes and ABS plastic. With the newly developed filament, they observed 40% and 60% increase in the tensile strength and Young's modulus of the 3D printed parts, respectively. Zhong et al. [31] incorporated short glass fibers into ABS matrix to produce FFF filament. Their results showed that the parts made of glass fiber reinforced filament feature higher tensile strength relative to pure ABS. In a more recent study, Ning et al. [21] investigated the mechanical performance of FFF 3D printed parts made of virgin carbon fiber reinforced ABS filament. ASTM D638 standard was followed to prepare tensile test specimens with different fiber content, i.e. 3, 5, 7.5, 10, and 15 wt%. Compared with the pure ABS specimens, an improvement in the flexural and tensile strength was attained by increasing the fiber content from 3 to 5 wt%. However, a further increase in the fiber content from 5 wt% to 10 wt% resulted in a reduction of the tensile strength. This reduction in properties is attributed to the pores that develop during the extrusion and printing process of the filaments with high fiber content. Stoof et al. [32] exploited the possibility of natural fiber reinforced Poly-propylene composites as a feedstock for 3D-printing. Their work particularly investigated the effect of fibers on the strength and shrinkage of the printed samples. The results showed that the tensile strength and Young's modulus of both the filament and the 3D printed samples have increased by 70% and 210%, respectively. It was also observed that increasing the fiber content has the potential to mitigate the shrinkage of the 3D printed objects.

While all the studies mentioned so far focused on the use of virgin fibers, only recently have scrap materials been used to develop FFF feedstock. For example, in an experimental study, a novel FFF filament based on PLA and Lecce Stone (LS) scraps was successfully designed and developed [33]. Although no mechanical study was performed, the study showed that the thermal degradation of the newly developed filament is similar to that of the conventional pure PLA filament, thus ensuring a high processability of the LS/PLA filament. In another study, nylone6 industrial waste,

Al_2O_3 and Al powder were used to achieve a filament featuring higher roughness and wear resistance relative to commercial FFF filament material [34].

The aim of this work is to use fiber glass scrap from wind turbine blades as reinforcement in thermoplastic filaments for 3D printing to achieve the following: addressing the challenging issue of wind turbine blade scrap that is increasingly growing every year; and improving mechanical properties of 3D printed thermoplastic parts without the need of adding high cost virgin fibers. In this paper, the ASTM D638 standard test method is followed to properly characterize tensile strength of 3D printed parts out of pure PLA and PLA reinforced with fiberglass. In the following sections, first, a systematic methodology is proposed integrating mechanical recycling and filament extrusion to manufacture PLA filaments reinforced with fiberglass. Then, specimen geometry, configuration, and testing procedure are described as per ASTM D638. Next, the specimen manufacturing, including 3D printing process and design parameters, is described extensively. Experimental testing is performed and the tensile strength for different filament materials is obtained. Finally, the performance of the 3D printed specimens with pure and reinforced PLA is discussed and recommendations for future research are presented.

2. Methodology

One of the causes of environmental pollution is landfill of wind turbine blades. This work proposes to recycle the turbine blades at their end-of-life and reincorporate them into thermoplastic FFF filaments. The cost analysis on the landfill of wind turbine blades has shown that it is presently the most economical feasible solution to dispose of the scrap blades. However, the EU directive on the landfill of waste, 1999/31/EC, prohibits the landfill of Glass Fiber Reinforced Plastics (GFRPs) and many countries are now imposing tax upon organic wastes, which are put into landfill [12]. Hence, despite the low cost of virgin glass fibers, the tighter environmental regulations that are sure to come, will enhance the economical long-term benefits for recycling GFRPs. The major aspects of the approach that are taken here rest on the integration of mechanical grinding and filament extrusion to transform the recycled glass fibers into commercial FFF feedstock material. Figure 1 depicts the current methodology, where the key steps are briefly described below:

1. A mechanical recycling method combining grinding and a double sieving process is performed to recover the glass fibers from the scrap blades. Since the diameter of the 3D printer nozzle used here is 0.4 mm, the double sieving operation ensures a supply of fibers with a length generally below 0.4 mm, a characteristic essential for filaments with high processability.
2. The mixture of the PLA pellets and the fibers are placed in a dehydrator machine for a drying process of 4 hours at 60ºC. This dehydrations process reduces the moisture content of the pellets that could generate voids during the extrusion process.
3. To generate the Recycled Glass Fiber Reinforced Filament (RGFRF) for FFF, the raw materials obtained in step 2 are first fed into a twin-screw extruder connected to a pelletizer to produce glass fiber reinforced pellets. Following the initial extrusion, the pellets are re-dried and fed into a single screw extruder to produce RGFRF. The extruder screw speed, the die temperature as well as the winder speed are tuned to attain a filament with consistent

diameter of 1.75 mm. A laser micrometer with an accuracy of ±2 µm is used along with the extruder to monitor the filament diameter.

4. Tensile properties of a single filament made out of pure PLA, as a baseline, and reinforced filaments are compared. In addition, tensile coupons are manufactured as per ASTM D638 type I out of pure PLA filament and RGFRF. Tensile testing is performed on the coupons and the resulting mechanical properties are compared to evaluate the performance of the newly developed filament.

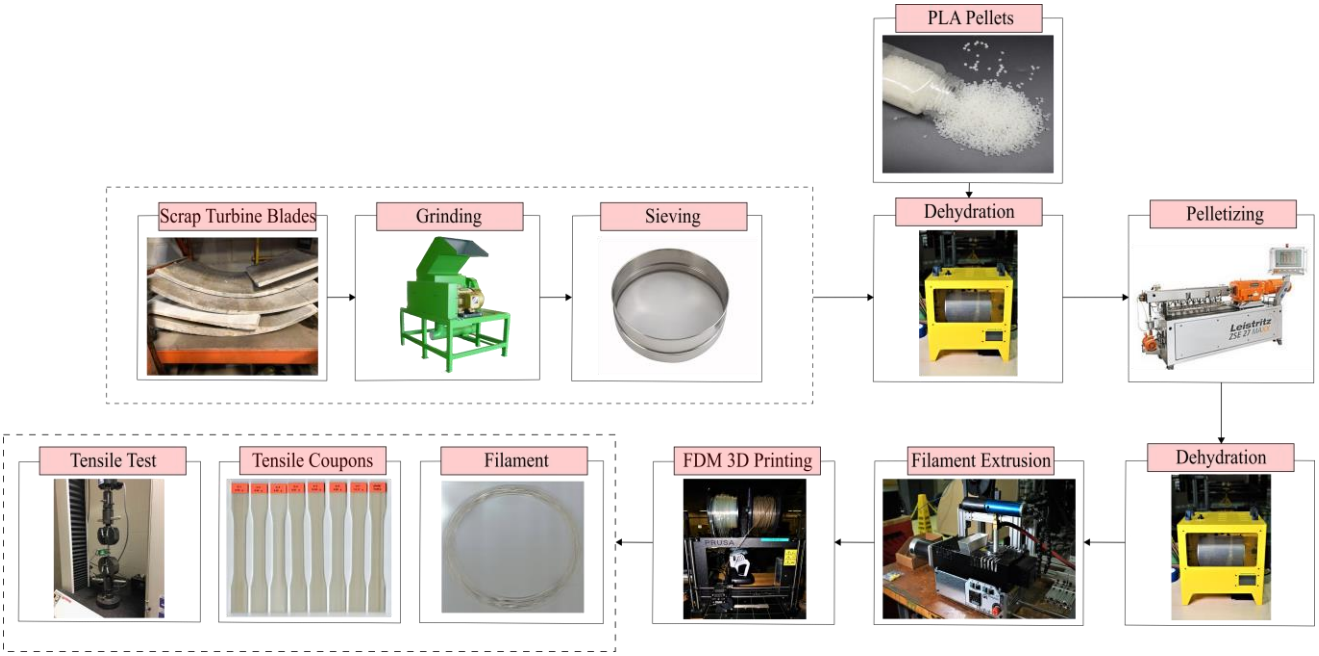

Figure 1: The proposed methodology for recycling of wind turbine blades.

2.1 Mechanical recycling

To avoid the consequences of landfill and incineration, one focus of this work is on the mechanical grinding of the rotor blades, a size reduction technique for a simple and fast recovery of the glass fibers from the scrap blades. Further, grinding with an impact and hammer mill has shown to be the most efficient way to reduce the size of glass fiber reinforced composites due to the abrasive nature of fiberglass [11]. In the present study, recycled glass fibers with an average length of 0.1-0.4 mm are obtained from grinding a turbine blade made of glass fiber reinforced epoxy composite. Since the nozzle diameter of the printer used in this investigation is 0.4 mm, this range of fiber length ensures a high processability for the proposed filament. Longer fiber lengths lead to the possibility of clogging the 3D printer output nozzle. As observed in Figure 2, a three-stage recycling procedure is used here to obtain the fibers for the filament extrusion: First, the blades are cut down into 20 × 20 cm pieces using a band saw and then fed into a grinder machine (ECO-WOLF, INC.) consisting of a hammer mill system and a classifier with a hole size of 3 mm. Following the first granulation process, visual inspection microscopy of the recycled materials demonstrates a mixture of resin powder and fibers, resulting in a fiber length range of 0.1-2.5 mm. To further classify the recycled materials, a double sieving mechanism is used and two grades of granulated material are obtained. The granulated blade obtained from the first grinding process is

sieved through a stainless-steel screen with a hole size of 0.1 mm. The larger-sized recycled material is then re-fed in the sieve for the second sieving operation to extract more fine fibers that are in the desirable length range.

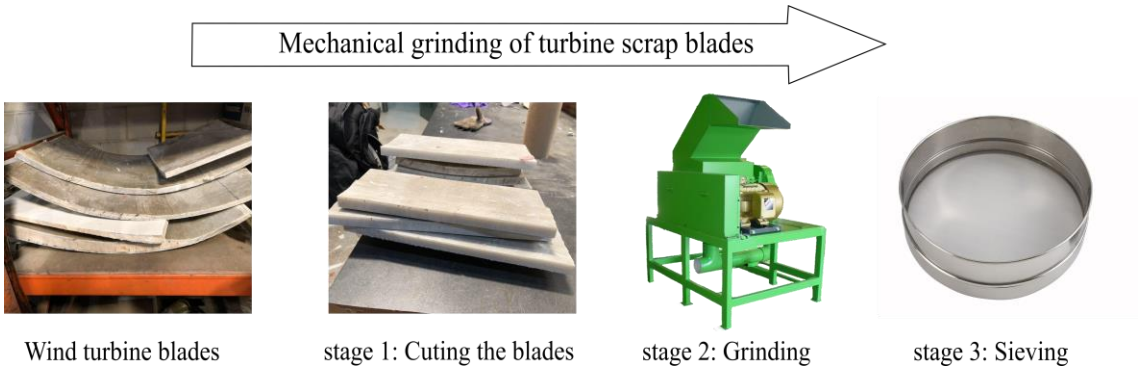

Figure 2: The proposed three-stage grinding methodology for the mechanical recycling of wind turbine blades.

2.2 Filament extrusion

The RGFRF was fabricated through a double melt extrusion process of PLA pellets (Ingeo 4043D, Natureworks LLC, Blair, Nebraska) and 5 wt% recycled glass fibers. PLA is a hygroscopic thermoplastic and readily absorbs moisture from the atmosphere. The presence of moisture will hydrolyze the biopolymer resulting in void generation during the extrusion process [35]. Furthermore, the presence of moisture on the surface of the fibers can form fiber clusters, which prevent a homogeneous distribution of fibers within the polymer. As a preventative measure, a dehydration process on the fibers and the PLA pellets is performed at 60 °C for 4 hours to dry the fibers and reduce the moisture content of the pellets to below 250 ppm. Once the fibers and the pellets are dried, we feed them into a twin-screw extruder (Leistritz ZSE18HP-40D, Nuremberg, Germany) with 8 subzones connected to a pelletizer to produce glass fiber reinforced pellets. This process ensures a homogeneous distribution of the fibers within the matrix, an essential factor to the dimensional accuracy of the filament, as well as the mechanical properties of the 3D printed components. The reinforced pellets are then re-dried and fed into a single screw extruder (FilaFab, D3D Innovations Limited, Bristol, UK) to produce RGFRF. To increase the dimensional accuracy of the filament, a spool winder machine is connected to the extruder, which allows for accurate control of the filament diameter. To consistently monitor the diameter of the filament, a laser micrometer with ±2 µm accuracy is used. The extrusion parameters including the screw speed, the speed of the winder as well as the die temperature are properly adjusted to achieve a 1.75 ± 0.05 mm filament, a suitable diameter and tolerance for the 3D printing process. The screw speed and the temperature of each zone during the initial and the second extrusion processes are reported in Table 1. Scanning Electron Microscopy (Hitachi UHR Cold-Emission FE-SEM SU8000) and optical microscopy (Nikon, Tokyo, Japan) are used to characterize the microstructural features of the RGFRF namely, the fiber distribution and fiber orientation. The filament is sectioned transversely and longitudinally, where the former is used to monitor the fiber distribution and the latter shows the fiber orientation. For the longitudinal cross section, the samples are potted in an epoxy resin, ground and polished in preparation for the

microstructural analysis. Grinding is done using 120 grit, followed by 220 and 600 grit sandpaper, and polishing is performed using a 10 µm diamond slurry, then a 5 µm diamond slurry, and finished with a 0.3 µm alumina suspension.

Table 1: The single and twin-screw extruders parameters.

Twin screw pelletizer	Screw speed (rpm)	90
	Subzone 1-2 (Temp °C)	190
	Subzone 3(Temp °C)	185
	Subzone 4(Temp °C)	180
	Subzone 5(Temp °C)	175
	Subzone 6-8(Temp °C)	170
	Screw speed (rpm)	25
Single screw filament maker	Die temperature (Temp °C)	210
	Winder speed (rpm)	1

To study the effect of the recycled fibers on the physical properties of the filament, in particular, the glass transition temperature and the crystalline content, DSC analysis is performed on the RGFRF and the pure PLA filament. Samples weighing in the range of 6-10 mg are extracted from the filaments and loaded into the DSC instrument (DSC Q100, TA Instruments, USA). The thermal history of the samples induced during the filament preparation is first removed with a heating procedure. Following the initial heating ramp, the samples are cooled down to ambient temperature at a rate of 5 °C /min and then held isothermally for 3 minutes. After the removal of the thermal history, the temperature is then ramped at a rate of 5 °C/min up to 200 °C to capture the glass transition temperature, as well as the melting peak of the samples. The DSC analysis is performed at least three times for each sample to verify the accuracy of the results.

The mechanical properties of the RGFRF, as well as the interface between the recycled fibers and PLA are assessed by performing tensile tests on both the RGFRF and the pure PLA filaments. A set of lifting thimbles with an inside diameter of 7/8 inch is used to clamp the filaments in the tensile machine. To ensure the validity of the results, the test is repeated five times and the average results are reported.

3. Specimens design and manufacturing

ASTM D638-14 standard is followed here to characterize the tensile properties of 3D printed parts made of RGFRF and pure PLA. As per ASTM D638, five different types of tensile test specimen are suggested. Type I is the preferred specimen for a thickness of less than 7 mm. Hence, type I is selected here, and a 3D model is created in SolidWorks (Dassault Systems, Waltham, MA) as per the geometry and dimensions given in the standard. Although manufacturing process and design parameters such as nozzle temperature, bed temperature, layer thickness and infill percentage play a major role in the structural performance of FFF 3D printed parts, in this work the influence of the feedstock material is studied. To do so, the manufacturing process and design parameters are kept identical for all the specimens and a relative comparison is performed based on their tensile properties. As a result, five pure PLA and reinforced specimens with a total thickness of 3.36 mm

and 0° raster orientation are prepared using a Prusa i3 Mk2S printer for the test. Manufacturing process and design parameters are summarized in Table 2. The mass value of the specimens is measured by a precision balance. Tensile tests on the 3D printed samples are conducted in a test machine (312 Q tensile machine, Testresources) with a 10 KN force transducer capacity and a 5 mm/min testing speed.

Table 2: Manufacturing and design parameters for specimen 3D printing.

Manufacturing parameter	Value	Manufacturing parameter	Value
Print direction	XYZ	Nozzle diameter (mm)	0.4
Raster angle	0	Nozzle temperature (°C)	215
Layer height (mm)	0.14	Cooling	No fan cooling
Bed temperature (°C)	60	Infill (%)	100
Print speed (mm/min)	2400	Filament diameter (mm)	1.75

4. Results and discussion

This section summarises the results from mechanical grinding, filament fabrication, and tensile testing of filaments and 3D printed specimens. Three sets of results are herein presented. The first describes the mechanical recycling of the scrap rotor blades. The second discusses the filament fabrication and its performance, namely tensile and physical properties. Finally, the third describes the mechanical properties of the 3D printed tensile coupons made of RGFRF, which are then compared to coupons made from the conventional pure PLA filament.

4.1 Mechanical grinding

The methodology described in Section 2.1 is applied here for the mechanical recycling of wind turbine blades. Approximately, 60 % of the ground recycled material has come out of the sieve and is usable for the 3D printing process. However, the remaining sieved residue could be either reground and used in the same recycling system or processed with larger nozzle diameters. Figure 3 illustrates the probability distribution of the fiber length evaluated by measuring the length of at least 300 fibers from each grade of granulated material. As seen, after the second sieve operation, most of the fibers feature lengths in the range of 0.15-0.18 mm, thus ensuring the processability of the fibers for the use in the FFF process. Although it is difficult to differentiate the fibers in terms of shape characteristics, it could be concluded from visual inspection that after the second sieve operation, fiber bundles are separated, and fibers are in a better refined state. Resin residue in the form of powder is also visible in the recyclate. In some sections of wind turbine blades, balsa wood is generally used as core to reduce the production costs. In the present study, only pure fiberglass sections of a rotor blade are used to recover the glass fibers. Therefore, no wood powder is present in the fiberglass compound and it includes only matrix powder and fiberglass. In particular, this work did not consider the effect of the wood powder on the properties of the 3D printing composite filament. In addition, the recovered fibers, featured a dimeter ranging between 16 – 20 µm, which represents the diameter of E-glass fiber, the most commonly type of glass fiber used in wind turbine blades.

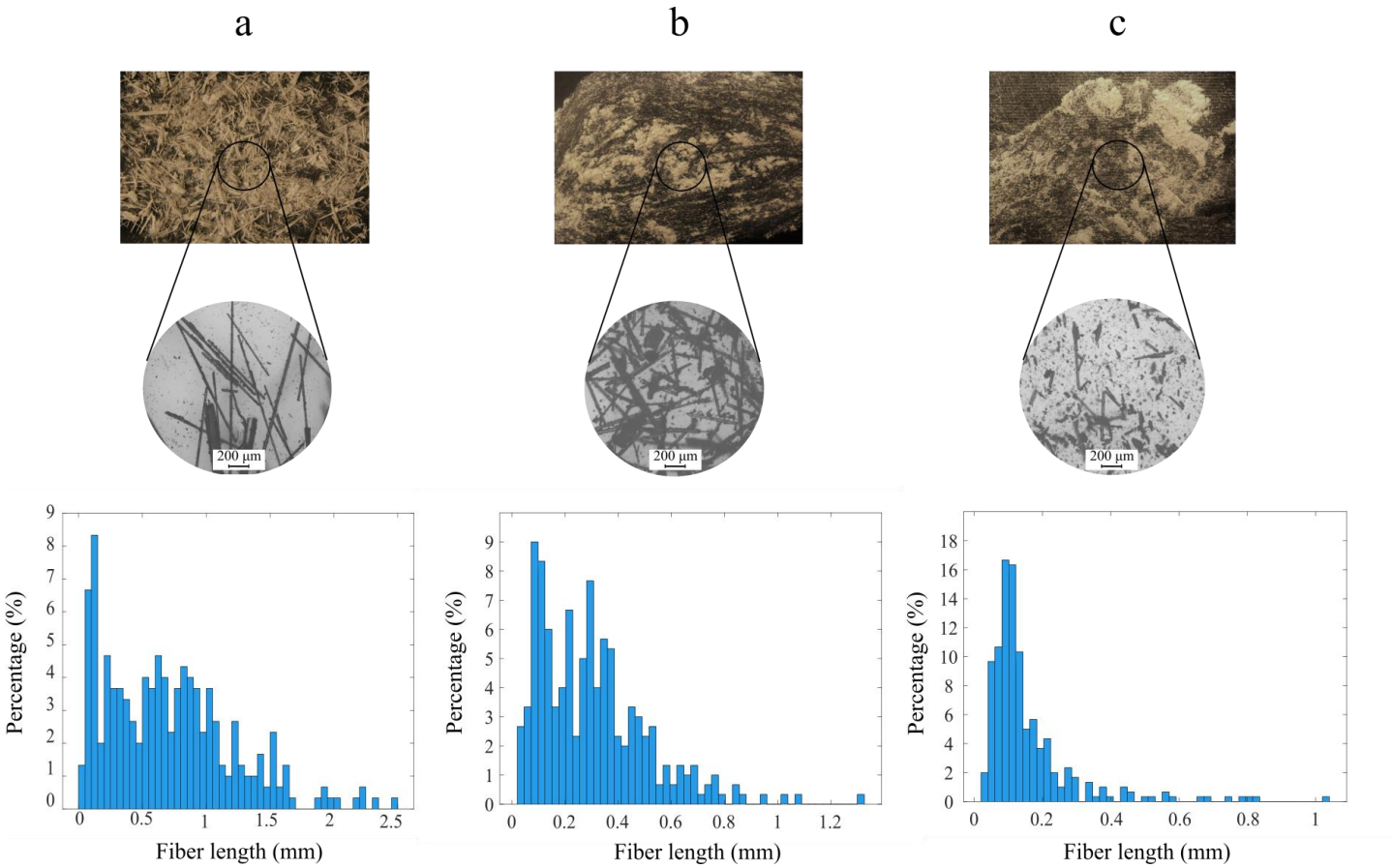

Figure 3:Probability distribution for fiber length of three grades of recycled fibers obtained from (a) grinding of blades; (b) first sieve operation; and (c) second sieve operation.

One of the main challenges that limits the use of the recycled fibers obtained from mechanical recycling, is traces of old resin, which might contribute to a weak interface between fibers and matrix. Wind turbine blades are generally made of glass fiber reinforced epoxy composites [36]. Figure 4 illustrates an example of the morphology of the recycled fibers. As seen, the epoxy residue still covers some parts of the surface of the fibers. The epoxy resin is characterised by the possession of more than one 1,2-epoxy groups per molecule, which are highly reactive with many substances, particularly those that are known as proton donors such as PLA [37]. This leads to the possibility of favorable interactions between functional groups of PLA and epoxy via hydrogen bonding. Such reactions allow for molecular chain extensions, which can improve the interfacial strength between the PLA and the recycled fibers without the need for expensive thermal or chemical treatment processes to remove the old resin. Further, the matrix residue on the surface of the fibers increases the fibers roughness, which could contribute to the mechanical interactions between the fibers and the PLA molecules.

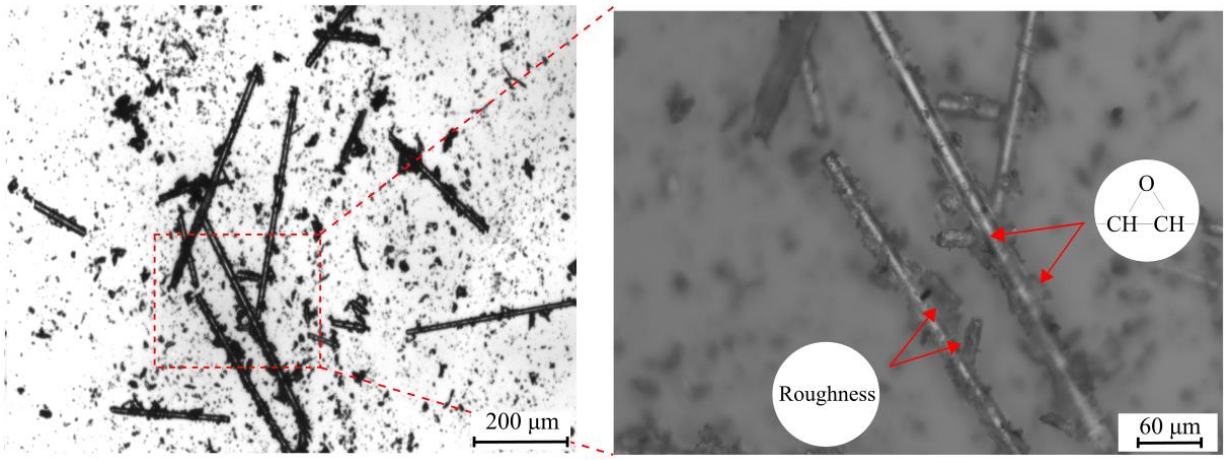

Figure 4: The residue of epoxy on the surface of the recycled fibers.

4.2 FFF 3D printing filaments

Figure 5 shows the pure PLA filament and RGFRF with 5% wt fiber content.

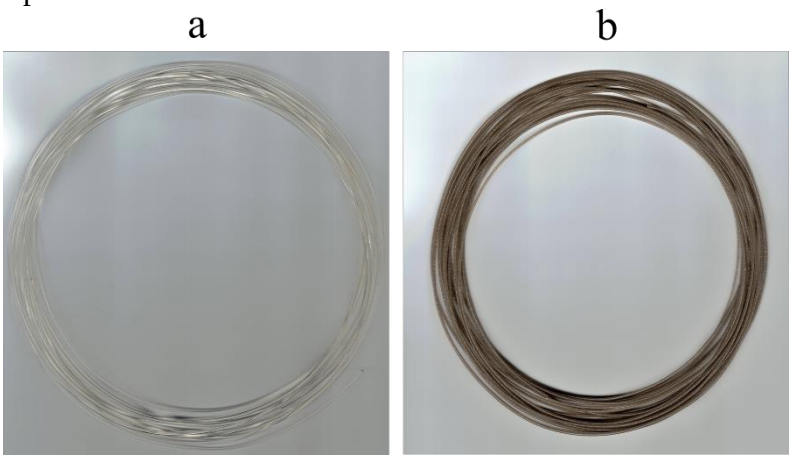

Figure 5: (a) The pure PLA filament; (b) the RGFRF with 5% fiber content.

A typical stress-strain curve for both the pure PLA filament and RGFRF, along with their tensile properties, are shown in Figure 6. The results demonstrate an increase of 10% in the Ultimate Tensile Strength (UTS) from 51.66 (σ = 0.58 and CV = 1.1%) to 56.63 (σ = 5.55 and CV = 9.8%) MPa and 16% in tensile modulus from 3.17 (σ = 0.1 and CV = 3.2%) to 3.6 (σ = 0.09 and CV = 2.5%) GPa for RGFRF relative to pure PLA filament. We recall that σ and CV represent the standard deviation and the coefficient of variation of the results, respectively. A larger variability is observed for the strength results of the reinforced composite filament, which could be ascribed to the diameter variations in the filament as well as, variations in the surface quality of the filament due to the presence of long fibers in the compound. On the other hand, the variability of the stiffness results for the composite filament is comparable to that of the pure PLA filament and all the samples showed higher stiffness relative to the pure PLA samples. The precise control of the filament diameter and carefully separating the fibers longer than the 3D printer nozzle diameter could result in lower variations in tensile strength.

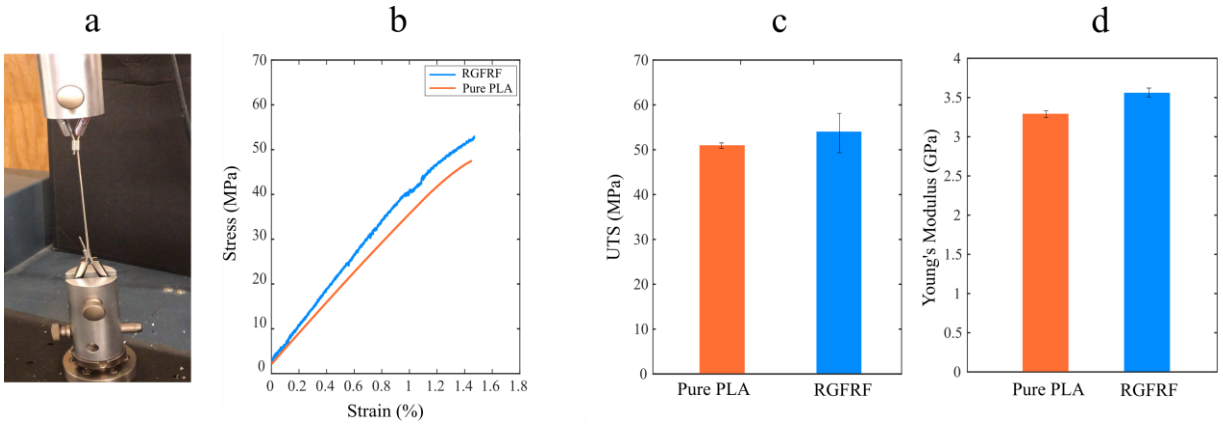

Figure 6: The tensile properties of the extruded pure PLA filament and reinforced filament: (a) test set-up; (b) stress-strain curve; (c) UTS; (d) Young's modulus.

The microstructures of the pure PLA filament and RGFRF along the transverse and longitudinal directions are shown in Figure 7. As it can be seen, the PLA filament shows smooth and round edges with no visible air bubbles, indicating the successful removal of the moisture content during the dehydration process. The RGFRF, on the other hand, contains relatively small internal voids that are distributed throughout the filament. The double extrusion process increases the likelihood of moisture absorption by the PLA and consequent air bubble formation probability during the extrusion process. As observed in the transverse cross section of RGFRF, glass fibers are visible in the reinforced filament and are well distributed throughout the cross section. The longitudinal cross section reveals that the fibers are generally well aligned in the directions of extrusion. This observation suggests that the RGFRF can be treated as a short glass fiber reinforced composite. Halpin-Tsai [38] has shown that the elastic modulus of short fiber reinforced composites along the fiber direction can be expressed as:

$$\frac{E_L}{E_m} = \frac{1 + (2l/d)\eta_L V_f}{1 - \eta_L V_f}, \tag{1}$$

$$\eta_L = \frac{E_f/E_m - 1}{\frac{E_f}{E_m} + 2(l/d)}, \tag{2}$$

where l represents fiber length, d is the fiber diameter, V_f is the volume fraction of the fibers, E_f is the elastic modulus of the fibers and E_m is the matrix modulus.

Based on the probability distribution analysis, the Young's modulus of RGFRF can be estimated assuming a uniform fiber length and fiber diameter of, respectively, 0.15 mm and 0.02 mm throughout the filament. The value of elastic stiffness for PLA and fiberglass is respectively 3.6 GPa and 72 GPa [39]. Therefore, the elastic stiffness of a short fiber reinforced composite with 5% wt fiber content can be predicted to be 4.3 GPa, which is larger than the average modulus observed for RGFRF. The discrepancy between the stiffness of RGFRF and the theoretical stiffness of short fiber reinforced composite can be attributed to the presence of voids, orientation of fibers within the filament structure, and variation in fiber length and filament diameter. The theoretical model of Halpin-Tsai indicates an elastic modulus 1.2 times greater than that of conventional PLA plastic. However, the average elastic modulus observed for the RGFRF is lower

than the predicted stiffness, at approximately 1.14 times the average stiffness of the pure PLA filament.

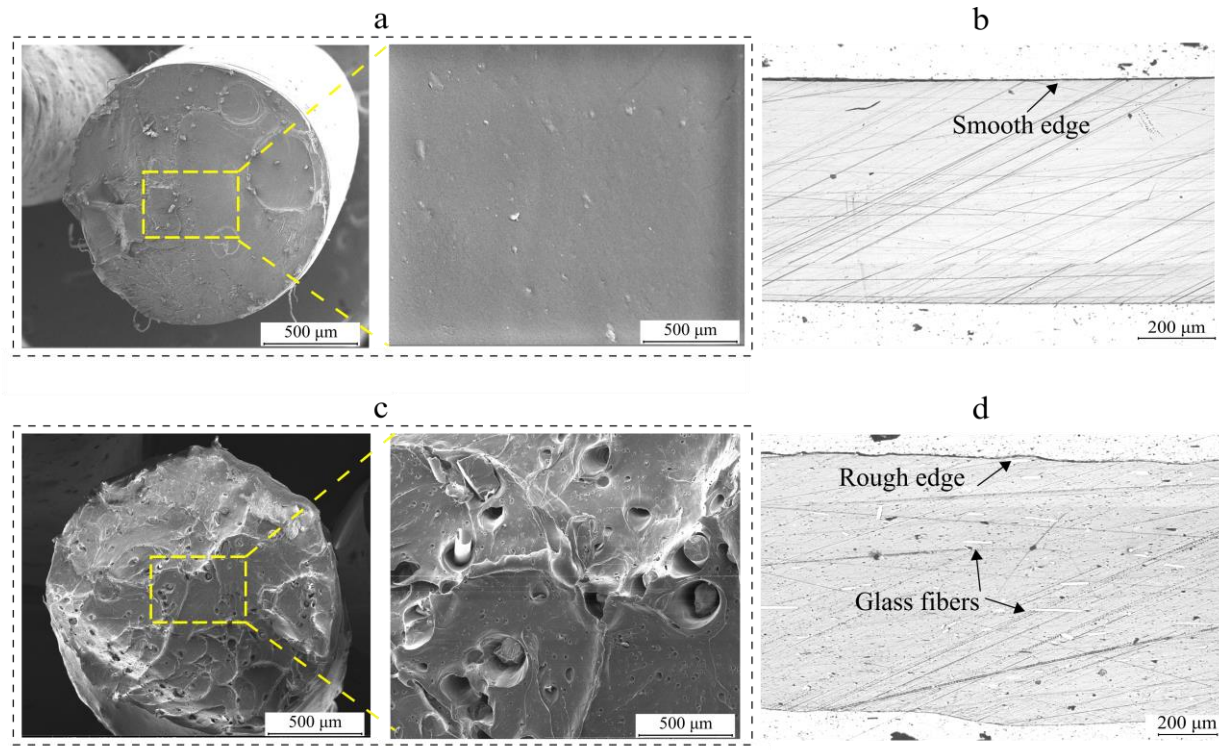

Figure 7: SEM images of pure PLA filament and RGFRF: (a) The transverse cross section of pure PLA filament; (b) the longitudinal cross section of pure PLA filament; (c) the transverse cross section of RGFRF; and (b) the longitudinal cross section of RGFRF.

The DSC curves shown in Figure 8 illustrate the heat flow versus the temperature scan of RGFRF and the pure PLA filament. The glass transition temperature of each filament is evaluated from the inflection point of the step transition using commercial software (TA Universal Analysis). The results are reported in Table 2. As seen, no significant change was observed in the glass transition temperature of RGFRF relative to the pure PLA baseline.

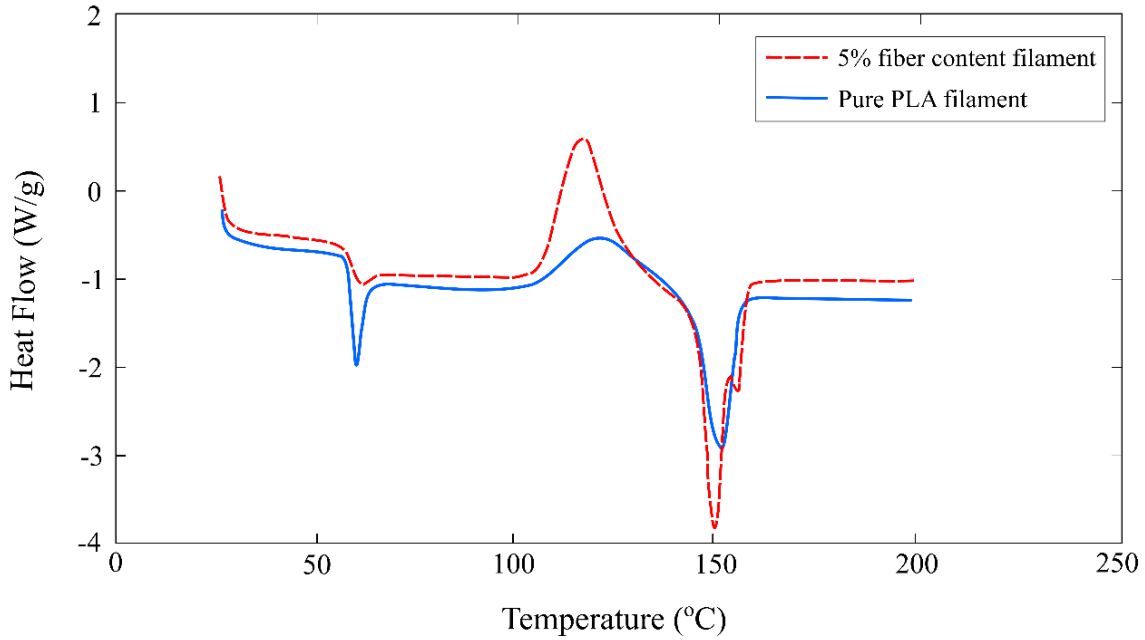

Figure 8: The DSC thermograms of the PLA filament and RGFRF.

To further investigate the effect of recycled glass fibers on the physical properties of the filament here introduced, we also computed its crystalline content and compared to that of the pure PLA baseline. The enthalpy of melt crystallisation represents the amount of crystalline content of a substance. As a result, the degree of crystallinity of a substance can be expressed as

$$\lambda_c = \frac{\Delta H_m - \Delta H_C}{\Delta H_f (1 - W_f)} \times 100, \quad (2)$$

where ΔH_m is the enthalpy of fusion, ΔH_C is the enthalpy of cold crystallisation, ΔH_f is the enthalpy of fusion of 100% crystalline PLA, which is selected to be 93.1 J/g [40], and W_f is the weight fraction of fibers in the polymer. Although low degree of crystallinity was observed for both samples, we observed that the reinforced filament is less amorphous as compared to pure PLA filament. The higher crystallinity of the reinforced filament could contribute to higher stiffness and lower degradation rate.

Table 2: The glass transition temperature and crystallinity of the pure PLA filament and RGFRF.

Specimen	T_g (°C)	T_m (°C)	$\Delta H_c\ (J/g)$	$\Delta H_m\ (J/g)$	λ_c (%)
Pure PLA	57.2	150.7	15.84	18.11	2.4
RGFRF	57.87	151.5	24.31	26.74	2.7

Another dominating property in the processability and performance of 3D printing filaments is the melt flow index, which is inversely proportional to viscosity. The viscosity of the RGFRF is evaluated by a rheometer (AR2000, TA instruments, USA) using a plate-plate configuration at 210 °C for shear rates ranging 0.01-10 1/s. The temperature used for the viscosity evaluation represents the temperature used in the 3D printing process. As illustrated in Figure 9, the results demonstrate a higher viscosity for the reinforced filament at low shear rates. However, as the shear rate increases, the links between the fibers and the PLA molecules break, leading to lower viscosity.

This suggests that at the shear rates used in the 3D printing process, the effect of fiberglass on the rheological properties of the filament is minimal and negligible.

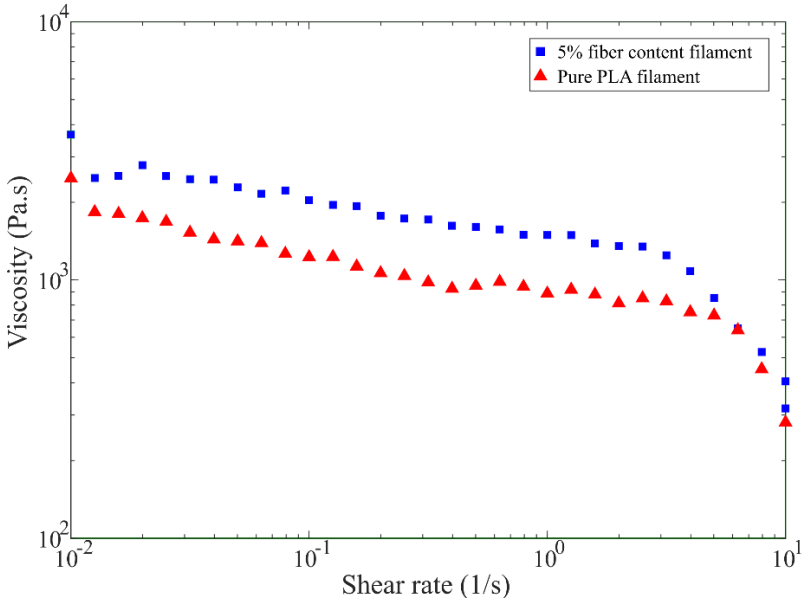

Figure 9: Rheological curves of the pure PLA filament and RGFRF.

4.3 FFF 3D printed coupons

The FFF 3D printed tensile test specimens are shown in Figure 10. The tensile test coupons are comprised of 24 layers with a unidirectional bead orientation.

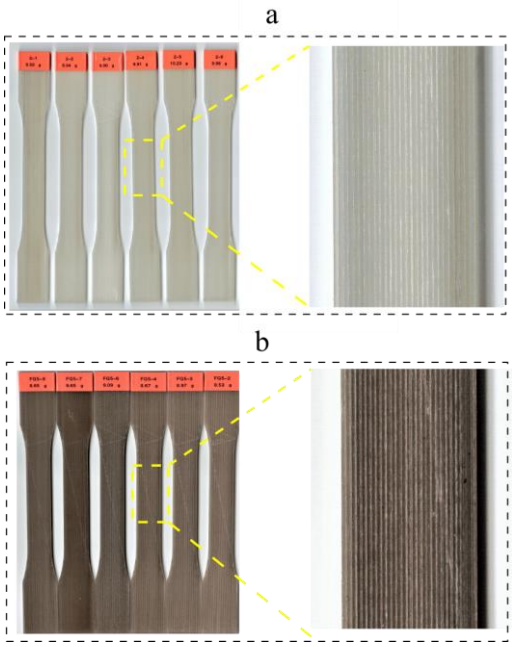

Figure 10: (a) the pure PLA tensile test coupons with unidirectional bead orientation; (b) the reinforced coupons with unidirectional bead orientation.

Figure 11 shows the representative engineering stress-strain curves for the tensile test samples. Due to diameter variations in the RGFRF, lower density values with respect to pure PLA samples were observed for the composite samples. To compensate for this, the UTS results of the composite samples are scaled-up with respect to the density of pure PLA specimens. It was observed that the 3D printed composite samples feature a Young's modulus enhanced by about 8% from 3.12 (σ = 0.15 and CV = 4.8%) to 3.35 (σ = 0.12 and CV = 3.6%) GPa compared with pure PLA specimens, while there was no meaningful increase in UTS. The elastic stiffness of the 3D printed specimens is slightly lower compared to the individual filaments, e.g. 1.5% and 7% reduction for pure PLA and composite coupons, respectively. The discrepancy between mechanical properties of the filaments and the coupons could be attributed to the 3D printing process that introduces some defects and higher quantity of large voids, e.g. interlayer voids, within the samples [2, 41, 42]. As observed in Figure 12, while a brittle failure plane normal to the load axis was observed in pure PLA samples, the composite specimens failed due to interlayer delamination and debonding of adjacent beads. This could be due to the presence of voids distributed throughout the long axis of the reinforced coupons, which causes the failure to evolve with the propagation of cracks along the beads. Such porosity distribution may be the cause of the low ultimate strength for the composite specimens. Moreover, this type of failure highlights the fiber bridging phenomena, which directs the crack propagation in the longitudinal direction.

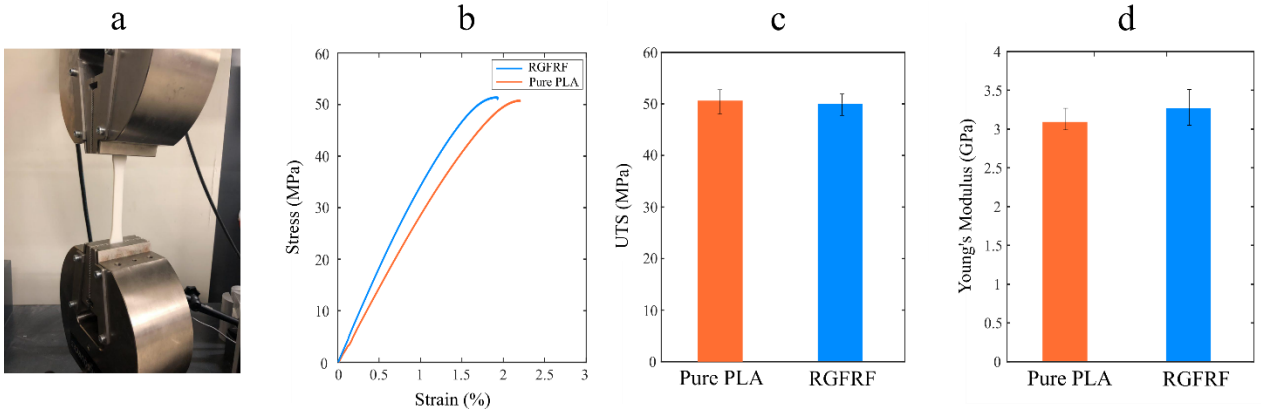

Figure 11: The tensile properties of the pure PLA and composite tensile test specimens: (a) test set-up; (b) stress-strain curve; (c) UTS; (d) Young's modulus.

To explore the porosity of the coupons, SEM images from the fracture surface of the pure PLA and reinforced specimens are examined. As seen in Figure 13, the reinforced samples feature larger internal voids, which are likely a result of nozzle clogging due to the presence of fibers with larger length compared to the nozzle diameter. The presence of ruptured fibers demonstrates an effective load transfer capacity between the PLA matrix and the recycled fibers. The SEM images show that some fibers have been pulled out of the PLA due to insufficient interfacial strength. This could be attributed to the variation of the epoxy residue on the fibers surface, which lowers the possibility of the molecular interactions and thus hydrogen bonding at the interface of the pulled-out fibers and PLA.

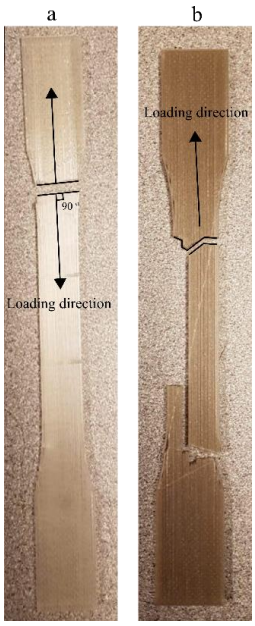

Figure 12: Failed samples: (a) pure PLA, and (b) recycled glass fiber reinforced PLA.

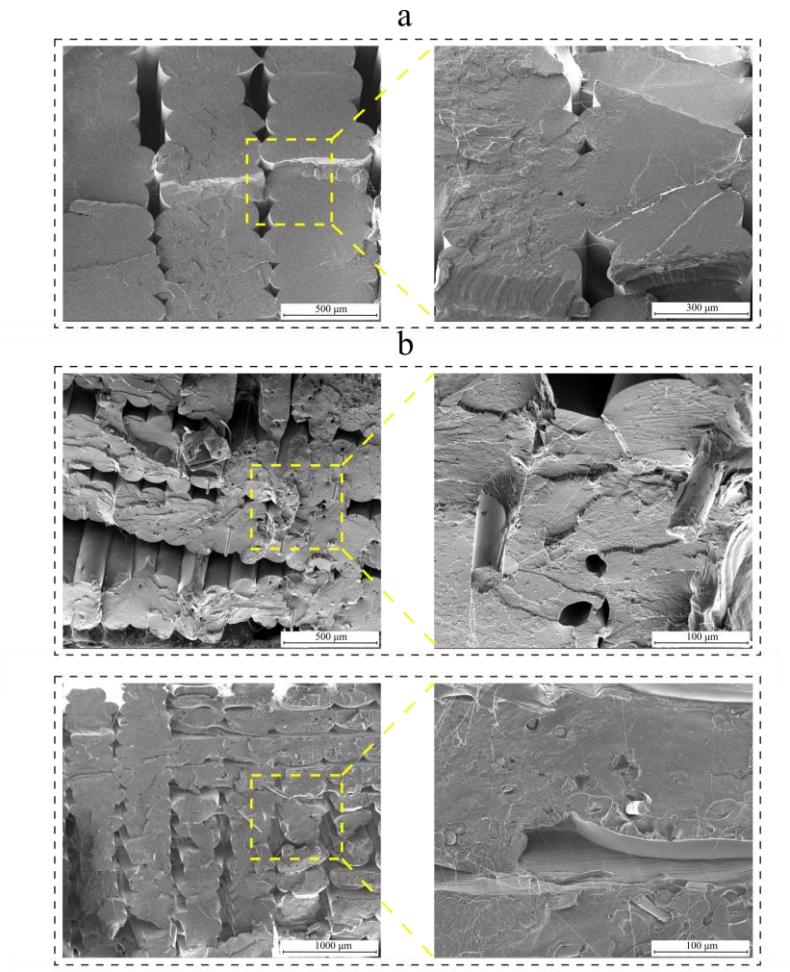

Figure 13: The fracture surface SEM of the 3D printed specimens: (a) pure PLA; and (b) with recycled glass fibers.

5. Conclusion

This study describes and validates a methodology integrating mechanical recycling and FFF 3D printing as a potential solution to the problem of composite waste from wind turbine blades. The scrap turbine blades are first ground and sieved to obtain processable recycled glass fibers for application in 3D printing. The ground fibers are then mixed with PLA, a biodegradable polymer, to extrude glass fiber reinforced filament. To demonstrate the mechanical performance of the newly developed filament, tensile test specimens with 5 wt% fiber content are fabricated and the effect on tensile properties, namely Young's modulus and tensile strength, are studied. The reinforced filament features a glass transition temperature comparable to that of pure PLA filament. However, a slight increase in the crystallinity of the reinforced filament is observed with respect to pure PLA filament. The results show that the addition of 5 wt% recycled fibers leads to an increase of 16% and 10% in the Young's modulus and strength of the pure PLA filament, respectively. Considering variability in tensile strength results, further experimental studies and larger sample sizes are required to validate potential improvements in strength.

Mechanical tests on FFF fabricated coupons demonstrate an increase of 8% in the Young's modulus relative to pure PLA samples, while there is no significant improvement in tensile strength. This level of performance would translate in the potential of application of recycled glass fibers from wind turbine blades into the 3D printing industry. SEM micrographs from the fracture surface of FFF composite samples show the presence of ruptured fibers confirming an effective load transfer between the PLA matrix and the recycled fibers. To better understand the interfacial strength between the recycled fibers and the thermoplastic matrix, further study is required to compare the interface of PLA with virgin and recycled fibers. Another aspect that requires further investigation is the effect of fiber content on the interfacial bonding and the mechanical properties of the 3D printed samples.

References

[1] Yang Y, Boom R, Irion B, van Heerden D-J, Kuiper P, de Wit H. Recycling of composite materials. Chemical Engineering and Processing: Process Intensification. 2012;51:53-68.
[2] Tian X, Liu T, Yang C, Wang Q, Li D. Interface and performance of 3D printed continuous carbon fiber reinforced PLA composites. Composites Part A: Applied Science and Manufacturing. 2016;88:198-205.
[3] Advani S, Hsiao K-T. Introduction to composites and manufacturing processes. Manufacturing Techniques for Polymer Matrix Composites (PMCs): Elsevier; 2012. p. 1-12.
[4] Campbell Jr FC. Manufacturing processes for advanced composites: Elsevier; 2003.
[5] Albers H, Greiner S, Seifert H, Kühne U. Recycling of wind turbine rotor blades–fact or fiction. DEWI Mag. 2009;34:32-41.
[6] Larsen K. Recycling wind turbine blades. Renewable energy focus. 2009;9(7):70-3.
[7] Job S. Recycling glass fibre reinforced composites–history and progress. Reinforced Plastics. 2013;57(5):19-23.
[8] Cherrington R, Goodship V, Meredith J, Wood BM, Coles SR, Vuillaume A, et al. Producer responsibility: Defining the incentive for recycling composite wind turbine blades in Europe. Energy Policy. 2012;47:13-21.
[9] Palmer J, Ghita OR, Savage L, Evans KE. Successful closed-loop recycling of thermoset composites. Composites Part A: Applied Science and Manufacturing. 2009;40(4):490-8.
[10] Oliveux G, Dandy LO, Leeke GA. Current status of recycling of fibre reinforced polymers: Review of technologies, reuse and resulting properties. Progress in Materials Science. 2015;72:61-99.
[11] MARTIN SA. Comparison of hammermill and roller mill grinding and the effect of grain particle size on mixing and pelleting.: Kansas State University; 1981.
[12] Group SM. Recycling of waste glass fiber reinforced plastic with microwave pyrolysis. 2012.
[13] Yang C, Tian X, Liu T, Cao Y, Li D. 3D printing for continuous fiber reinforced thermoplastic composites: mechanism and performance. Rapid Prototyping Journal. 2017;23(1):209-15.
[14] Greco A, Maffezzoli A. Rotational molding of biodegradable composites obtained with PLA reinforced by the wooden backbone of opuntia ficus indica cladodes. Journal of Applied Polymer Science. 2015;132(48).
[15] Gray IV RW, Baird DG, Helge Bøhn J. Effects of processing conditions on short TLCP fiber reinforced FDM parts. Rapid Prototyping Journal. 1998;4(1):14-25.
[16] Gray IV RW, Baird DG, Bøhn JH. Thermoplastic composites reinforced with long fiber thermotropic liquid crystalline polymers for fused deposition modeling. Polymer composites. 1998;19(4):383-94.
[17] Mueller B. Additive manufacturing technologies–Rapid prototyping to direct digital manufacturing. Assembly Automation. 2012;32(2).
[18] Wong KV, Hernandez A. A review of additive manufacturing. ISRN Mechanical Engineering. 2012;2012.
[19] Stampfl J, Hatzenbichler M. Additive manufacturing technologies. CIRP Encyclopedia of Production Engineering: Springer; 2014. p. 20-7.
[20] Horn TJ, Harrysson OL. Overview of current additive manufacturing technologies and selected applications. Science progress. 2012;95(3):255-82.
[21] Ning F, Cong W, Qiu J, Wei J, Wang S. Additive manufacturing of carbon fiber reinforced thermoplastic composites using fused deposition modeling. Composites Part B: Engineering. 2015;80:369-78.

[22] Dudek P. FDM 3D printing technology in manufacturing composite elements. Archives of Metallurgy and Materials. 2013;58(4):1415-8.
[23] Tekinalp HL, Kunc V, Velez-Garcia GM, Duty CE, Love LJ, Naskar AK, et al. Highly oriented carbon fiber–polymer composites via additive manufacturing. Composites Science and Technology. 2014;105:144-50.
[24] Novakova-Marcincinova L, Novak-Marcincin J, Barna J, Torok J. Special materials used in FDM rapid prototyping technology application. Intelligent Engineering Systems (INES), 2012 IEEE 16th International Conference on: IEEE; 2012. p. 73-6.
[25] Turner BN, Gold SA. A review of melt extrusion additive manufacturing processes: II. Materials, dimensional accuracy, and surface roughness. Rapid Prototyping Journal. 2015;21(3):250-61.
[26] N. Turner B, Strong R, A. Gold S. A review of melt extrusion additive manufacturing processes: I. Process design and modeling. Rapid Prototyping Journal. 2014;20(3):192-204.
[27] Esposito Corcione C, Gervaso F, Scalera F, Montagna F, Sannino A, Maffezzoli A. The feasibility of printing polylactic acid–nanohydroxyapatite composites using a low-cost fused deposition modeling 3D printer. Journal of Applied Polymer Science. 2017;134(13).
[28] Kuo C-C, Liu L-C, Teng W-F, Chang H-Y, Chien F-M, Liao S-J, et al. Preparation of starch/acrylonitrile-butadiene-styrene copolymers (ABS) biomass alloys and their feasible evaluation for 3D printing applications. Composites Part B: Engineering. 2016;86:36-9.
[29] Nikzad M, Masood S, Sbarski I. Thermo-mechanical properties of a highly filled polymeric composites for fused deposition modeling. Materials & Design. 2011;32(6):3448-56.
[30] Shofner M, Lozano K, Rodríguez-Macías F, Barrera E. Nanofiber-reinforced polymers prepared by fused deposition modeling. Journal of applied polymer science. 2003;89(11):3081-90.
[31] Zhong W, Li F, Zhang Z, Song L, Li Z. Short fiber reinforced composites for fused deposition modeling. Materials Science and Engineering: A. 2001;301(2):125-30.
[32] Stoof D, Pickering K. Sustainable composite fused deposition modelling filament using recycled pre-consumer polypropylene. Composites Part B: Engineering. 2018;135:110-8.
[33] Corcione CE, Palumbo E, Masciullo A, Montagna F, Torricelli MC. Fused Deposition Modeling (FDM): An innovative technique aimed at reusing Lecce stone waste for industrial design and building applications. Construction and Building Materials. 2018;158:276-84.
[34] Singh S, Singh R. Experimental investigations for use of nylon6 industrial waste as FDM feedstock filament for investment casting applications. 2016.
[35] NatureWorks. Crystallizing and Drying Ingeo Biopolymer.
[36] Mishnaevsky L, Branner K, Petersen HN, Beauson J, McGugan M, Sorensen BF. Materials for Wind Turbine Blades: An Overview. Materials (Basel, Switzerland). 2017;10(11).
[37] Brydson JA. 26 - Epoxide Resins. In: Brydson JA, editor. Plastics Materials (Seventh Edition). Oxford: Butterworth-Heinemann; 1999. p. 744-77.
[38] Sung N. Analysis and performance of fiber composites, Second Ed., by Bhagwan D. Agarwal and Lawrence J. Broutman, Wiley, New York, 1990, 449 pp. Price: $59.95. Journal of Polymer Science Part A: Polymer Chemistry. 1991;29(12):1835-.
[39] NatureWorks. Ingeo™ Biopolymer 4043D Technical Data Sheet, 3D Printing Monofilament – General Purpose Grade.
[40] Ivey M, Melenka GW, Carey JP, Ayranci C. Characterizing short-fiber-reinforced composites produced using additive manufacturing. Advanced Manufacturing: Polymer & Composites Science. 2017;3(3):81-91.
[41] Gunaydin K, S. Türkmen H. Common FDM 3D Printing Defects2018.

[42] Calvert P. Freeform Fabrication. In: Buschow KHJ, Cahn RW, Flemings MC, Ilschner B, Kramer EJ, Mahajan S, et al., editors. Encyclopedia of Materials: Science and Technology. Oxford: Elsevier; 2001. p. 3340-7.